

Thermal degradation kinetics study and thermal cracking of waste cooking oil for biofuel production

Fekadu Mosisa Wako¹ · Ali Shemshedin Reshad¹ · Vaibhav V. Goud¹

Received: 26 June 2017 / Accepted: 5 October 2017 / Published online: 23 October 2017
© Akadémiai Kiadó, Budapest, Hungary 2017

Abstract Thermal cracking of waste cooking oil (WCO) for production of liquid fuel has gained special interest due to the growing demand of renewable fuel, depleting fossil fuel reserves and environmental issues. In the present work, thermal cracking of WCO to produce liquid hydrocarbon fuels without any preprocessing has been studied. Moreover, non-isothermal kinetics of WCO using thermogravimetric analysis (TGA) has been studied under an inert atmosphere at various heating rates. According to TGA result, active thermal decomposition of WCO was found to be between 318 and 500 °C. Furthermore, the temperature at which the maximum mass loss rate attained was shifted to higher values as the heating rates increased from 10 to 50 °C min⁻¹ and the values were found to be approximately similar to that of R_{50} . Besides, model-free iso-conversion kinetic methods such as Friedman (FM), Kissinger–Akahira–Sunose (KAS) and Flynn–Wall–Ozawa (FWO) were used to determine the activation energies of WCO degradation. The average activation energy for the thermal degradation of WCO was found to be 243.7, 211.23 and 222 kJ mol⁻¹ for FM, KAS and FWO kinetic methods, respectively. Additionally, the cracking of WCO was studied in a semi-batch reactor under an inert atmosphere and the influences of cracking temperature, time and heating rates on product distribution were investigated. From the reaction, an optimum yield of 72 mass% was obtained at a temperature of 475 °C, time of 180 min and a heating rate of 10 °C min⁻¹. The physicochemical properties studied were in accordance with ASTM standards.

Keywords Waste cooking oil · Thermal cracking · Organic liquid product · Thermogravimetric analysis · Kinetic analysis · Activation energy

Introduction

The gradual depletion of fossil fuels and moreover, the gradual increase in energy demand have stimulated interest in alternative sources of energy over the last few decades [1]. Moreover, the consumption of fossil fuels has been causing serious environmental pollution by generating carbon dioxide and leading to greenhouse effects [1]. Waste cooking oil (WCO) is a cheap and renewable source for fuel production, and hence its utilization makes it a prudent source for production of biofuel [2]. In biofuel production, more than 80% of the overall cost belongs to feedstock [3]. Hence, utilization of waste vegetable oils as a feedstock not only resolves the economics of biofuels, but also contributes a lot to the reduction in waste disposal [4]. Biofuels are liquid or gaseous fuels that can be generated from renewable sources [5]. The production of biofuels follows numerous routes depending on the type of feed and final product [2]. These routes can be thermochemical conversions (pyrolysis/thermal cracking, combustion, gasification) and biochemical methods [6]. Thermal cracking is one of the likely routes which produces biofuels that are analogous to petroleum derivatives [7, 8].

To understand the features of thermal cracking and to compute kinetic parameters, kinetic studies become a vital tool [9–14]. Currently, the application of thermo-analytical techniques such as thermogravimetric analysis (TGA) and differential thermogravimetry (DTG) under non-isothermal condition are popularizing in this respect. TGA gives mass loss as a function of time and temperature. The mass loss

✉ Vaibhav V. Goud
vvgoud@iitg.ernet.in

¹ Department of Chemical Engineering, Indian Institute of Technology Guwahati, Guwahati, Assam 781039, India

data generated from TGA are the important source to investigate the thermal degradation of different materials [15–19]. The rate of mass loss of a sample is predicted from the first derivative of TG and is proportional to the area under the curve [20]. The most important parameters that affect the degradation behavior of oil samples are heating rates, amount of sample, atmospheric condition (reactive or inert) and final decomposition temperature. Moreover, different kinetic models have been developed by several researchers [21–27] to compute kinetic parameters based on TGA data. In the present study, thermal degradation kinetics of WCO sample was investigated using various iso-conversional methods such as Friedman (FM), Flynn–Wall–Ozawa (FWO) and Kissinger–Akahira–Sunose (KAS) methods which are widely used to calculate the activation energy of degradation of different vegetable oils [28]. Further, thermal cracking of the sample in a laboratory-scale semi-batch reactor was studied to understand the effect of process parameters on the yield of organic liquid product (OLP).

Materials and methods

Materials

WCO was collected from Indian Institute of Technology Guwahati student cafeteria, Assam, India. After simple filtration process, the WCO passed through anhydrous sodium sulfate to remove the traces of water. The pre-treated WCO showed the acid value of 3 mg KOH g⁻¹ and density 752 kg m⁻³. The main fatty acids present in WCO are myristic acid (C_{14:0}): 0.5%, palmitic acid (C_{16:0}): 20.4%, stearic acid (C_{18:0}): 4.8%, oleic acid (C_{18:1}): 52.9%, linoleic acid (C_{18:2}): 13.5%, linolenic acid (C_{18:3}): 0.8% and eicosanoic acid (C_{20:0}): 0.3% [29]. Chemicals such as deuterated chloroform (CDCl₃) and methanol [CH₃OH (HPLC grade)] were purchased from Sigma-Aldrich Pvt. Ltd., India.

Thermal cracking

Thermogravimetric analysis (TGA) of WCO was conducted using thermogravimetric analyzer (*Model no: TGA 851e/LF/1100*). Approximately, 10 mg of WCO sample was used for each experiment. The temperature was raised from 30 to 800 °C at various heating rates (10, 20, 30, 40 and 50 °C min⁻¹) under an inert atmosphere. The flow rate of the gas (99.99% purity N₂) was maintained at 60 mL min⁻¹.

Further, laboratory-scale thermal cracking of WCO was carried out in a semi-batch reactor (250 mL capacity). For each experiment, 30 g of WCO was placed inside the

reactor under a constant flow of gaseous nitrogen with a flow rate of 60 mL min⁻¹. The reactor was heated externally by an electric furnace with PID controller to achieve final temperature of 400, 425, 450, 475 and 500 °C, at heating rates of 10 and 20 °C min⁻¹ and kept under isothermal conditions for the duration of 60–300 min. A condenser connected with flask was assembled to collect condensable vapor (i.e., OLP) in the flasks (Fig. 1). The yield of product was calculated using (Eq. 1)

$$\text{Yield of OLP (mass\%)} = \left(\frac{\text{Mass of OLP collected}}{\text{Mass of feed}} \right) \times 100\% \quad (1)$$

Characterization of WCO and OLP

Some of the physicochemical properties such as density, kinematic viscosity and calorific value of WCO and OLP were estimated using standard ASTM methods. Specific gravity bottles of 25 mL were used to measure the volume of sample, and density was calculated as the ratio of mass to volume of a sample. On the other hand, the viscosity of the fuel is an important property that affects spray properties of the fuel which in turn affect engine performance. Kinematic viscosity was measured using U-tube viscometer. It was calculated by multiplying measured average time with a constant of U-tube viscometer. The average time is the time at which a known volume of liquid flowing under gravity to pass through a calibrated glass capillary viscometer tube [30]. The calorific values of WCO and OLP were determined using bomb calorimeter in which 0.5–1 g of samples was placed in the bomb calorimeter crucible. When the temperature becomes constant, the bomb was fired and the rise in temperature was recorded to calculate calorific value according to ASTM D 2015-85. Flash point was determined by pouring about 100 mL of

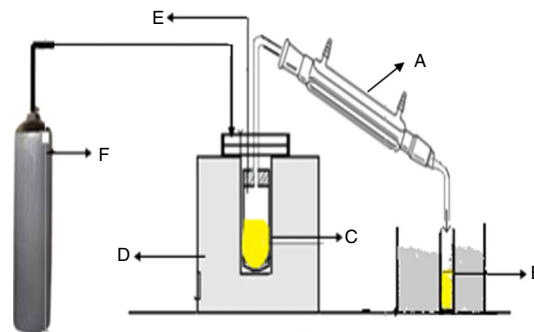


Fig. 1 Thermal cracking setup; *Notations: A: condenser, B: OLP yield, C: feed, D: furnace, E: reactor temperature, F: nitrogen gas*

the samples into the flash cup, and the lighted test flame was passed along the circumference of the cup. When a flash appeared at any point on the surface of the sample, the temperature was recorded, and that temperature was considered as a flash point according to ASTM D 92.

Fourier-transform infrared spectroscopy (FTIR) (*Shimadzu Model: IRAffinity1*) was used for identification of functional groups present in WCO and OLP with the aid of attenuated total reflectance (ATR). Approximately, 10 mg of the samples was injected on ATR crystal and the spectra were generated by the computer software in the range of wave number 400–4000 cm^{-1} . FTIR spectra of the samples were used for further analysis.

Nuclear magnetic resonance spectrometer analyses (NMR) of WCO and OLP were performed on *Bruker Ascend™* 600 MHz. Approximately, 10 mg of each sample was mixed with deuterated chloroform (CDCl_3), and the mixture was placed in the NMR tube. The OLP sample used in the chromatographic analysis was obtained under optimum reaction parameters of temperature 475 °C, residence time 120 min, catalyst loading 4 mass% and heating rate 10 °C min^{-1} . The chemical shifts are reported in ppm, using solvent proton signal as standard. The chemical shift of CDCl_3 observed at 7.2 ppm was taken as a reference. Further, gas chromatography–mass spectroscopy (GC–MS) (*Model no: 450-GC, 240-MS; Make: M/s Varian*) was used for identification of organic fractions present in the OLP sample. A capillary column (VF-5 ms) of 50 m \times 0.2 mm (0.33 μm film thickness) dimension was used. About 1 μL of the sample was introduced manually using a syringe into a gas chromatograph for analysis. Nitrogen was used as a carrier gas, and the following temperature program was set up for analysis. The oven was heated from temperature 70 °C (2 min) to 300 °C (7 min) at a heating rate of 10 °C min^{-1} to an injector temperature of 250 °C and holding time of 3 min. The identification of chemical compounds was performed on GC–MS, and the generated mass spectrum (peaks) was matched with a National Institute of Standards and Technology (NIST) research library.

Kinetic parameter calculation

The thermal decomposition rate of the sample could be expressed by considering Arrhenius temperature dependency at a constant heating rate using Eq. 2 [31]. The activation energy (E) for thermal decomposition of WCO was calculated using a model-free approaches such as Friedman (FM) (Eq. 5) [27], Flynn–Wall–Ozawa (FWO) (Eq. 7) [22] and Kissinger–Akahira–Sunose (KAS) (Eq. 6) [21] methods. For all methods, numerous TGA curves at different heating rates for the same value of conversion were used to determine the activation energy.

$$\frac{d\alpha}{dt} = \frac{A}{\beta} \exp\left(-\frac{E}{RT}\right) f(\alpha) \quad (2)$$

where β , $f(\alpha)$, A , α , E , T and R refer to a heating rate ($^{\circ}\text{C min}^{-1}$), reaction mechanism model, pre-exponential factor (1 min^{-1}), degree of decomposition of the samples, activation energy (kJ mol^{-1}), temperature (K) and gas constant ($8.314 \text{ J mol}^{-1} \text{ K}^{-1}$), respectively. The value of α at appropriate time/temperature was calculated using TG data (Eq. 3)

$$\alpha = \left(\frac{M_o - M_t}{M_o - M_{\infty}}\right) \quad (3)$$

$$\beta = \frac{dT}{dt} \quad (4)$$

where α is the mass loss fraction, M_o is the initial mass of the sample, M_t is the mass of a sample at time t , M_{∞} is the final, non-decomposable mass of the sample after the complete pyrolysis reaction.

FM is a differential iso-conversional method and is directly based on (Eqs. 2, 4) and its natural logarithm to obtain Eq. 5.

$$\ln\left(\frac{d\alpha}{dt}\right)_{ij} = \ln\left(Af(\alpha)_{ij}\right) - \frac{E_i}{RT_{ij}} \quad (5)$$

where i, j represent α and β , respectively. Different degrees of conversion (α) from 0.1 to 0.9 with 0.1 increments were considered to estimate E from the slope of $\ln\left(\frac{d\alpha}{dt}\right)_{ij}$ versus $\frac{1}{T_{ij}}$ curve.

KAS method is generated from Coats–Redfern approximation [21]. The general expression for n th-order thermal decomposition of sample is as follows (Eq. 6),

$$\ln\left(\frac{\beta}{T^2}\right)_{ij} = \ln\left(\frac{AR}{E_g(\alpha)_{ij}}\right) - \frac{E_i}{RT_{ij}} \quad (6)$$

The plot $\ln\left(\frac{\beta}{T^2}\right)$ versus $\frac{1}{T}$ at the value of α was a straight line with slope $-\frac{E}{R}$.

FWO method is a model-free iso-conversion method. The fundamental expression (Eq. 2) was also used by an integral method of FWO (Eq. 7) using Doyle approximation [22].

$$\ln(\beta_{ij}) = \ln\left(\frac{AE_i}{R_g(\alpha)_{ij}}\right) - 5.331 - 1.052 \frac{E_i}{RT_{ij}} \quad (7)$$

Similar to FM, for different conversion (α) the plot $\ln(\beta)_{ij}$ versus $\frac{1}{T_{ij}}$ is a straight line with a slope for a variable value of α which is a straight line whose slope is $-1.052 \frac{E}{R}$ and E was calculated from the slope of a line.

Results and discussion

Thermogravimetric analysis (TGA)

The thermal decomposition process of WCO was investigated in the temperature range of 30–800 °C at heating rates of 10, 20, 30, 40 and 50 °C min⁻¹ (Fig. 2a). The thermal decomposition of WCO at various heating rates (10, 20, 30, 40 and 50 °C min⁻¹) showed similar degradation pattern with less than 1% residue remained at around 530 °C (Fig. 2a). The main thermal degradation of the sample occurred in the temperature region of 318–500 °C and essentially completed in this zone. The behavior of a thermogravimetric curve with the corresponding DTG peaks gives a clear indication of the number of stages of thermal degradation [28]. Considering a single heating rate (i.e., 10 °C min⁻¹), the thermal decomposition of WCO occurred in the temperature range of 318–500 °C (96.5 mass%). With an increase in the heating rate from 10 to 50 °C min⁻¹, the rate of mass loss (5.3 mass% min⁻¹) was proximately same in the temperature range 318–500 °C. It can also be noticed that increase in the heating rate did not alter the pattern of the thermal decomposition; rather, it shifted the TG curve of WCO degradation to a higher temperature. The slope change on TG and DTG curve indicates the beginning of new step for a thermal degradation sample. Hence, it can be observed that the thermal decomposition of WCO took place in a single stage with similar degradation trends as that of at multi-heating rates (Fig. 2). But, peak temperatures (the rate at which maximum degradation occurred) for the thermal degradation of the samples were varying in their position. This may be because the heating rate is the significant factor on the thermal decomposition of the sample [28]. With an increase in the heating rate from 10 to 50 °C min⁻¹, the maximum rate of mass loss was increased from 17.56 to 96.15% min⁻¹ and also the

temperature at which maximum mass loss fraction occurred was shifted from 418.5 to 452 °C (Table 1). Similarly, the initial temperature (T_{onset}) and the final temperature (T_{offset}) for the thermal decomposition of WCO sample were shifted from 318.7 to 362.4 and 478.7 to 496.6 °C, respectively. R_{50} (the rate at which 50% mass loss) is the measure of the reactivity of samples for the thermal decomposition of the WCO. The values were found to be 17, 38.5, 54 and 73 and 96.5 mass% min⁻¹ at temperatures of 420, 432, 439, 445 and 452 °C at heating rate of 10 °C min⁻¹, 20, 30, 40 and 50 °C min⁻¹, respectively. Generally, the temperature at which rate of mass loss is maximum (M_{max}) was found to be proximity similar to that of R_{50} .

Kinetic analysis

Figure 3a–c shows the iso-conversional plots of FM, KAS and FWO at heating rates of 10, 20, 30, 40 and 50 °C min⁻¹, respectively. Figures indicate that the fitted lines are parallel at different conversions (0.1–0.9) and heating rates (10–50 °C min⁻¹). From the plots, the activation energies for the selected conversion (α) were calculated from the slope of the line (Fig. 3a–c) and obtained values are summarized in Table 2. The values of activation energies obtained were within the range of 212.5–295 kJ mol⁻¹ (FM), 161–255 kJ mol⁻¹ (KAS) and 172–267 kJ mol⁻¹ (FWO). Higher correlation coefficients (R^2) obtained for all methods showed fitness of the model. The activation energy values (Fig. 3d) found to be increased with an increase in the conversion for KAS and FWO methods, but the fluctuation in the activation energy value was observed in FM method which might be because of mathematical errors associated with the method. The mean values of activation energies were found to be 243.7 kJ mol⁻¹ (FM), 211.3 kJ mol⁻¹ (KAS) and 222 kJ mol⁻¹ (FWO). It can be seen from (Table 2) that

Fig. 2 TGA (a) and DTG (b) curve of WCO decomposition at heating rates of 10, 20, 30, 40 and 50 °C min⁻¹

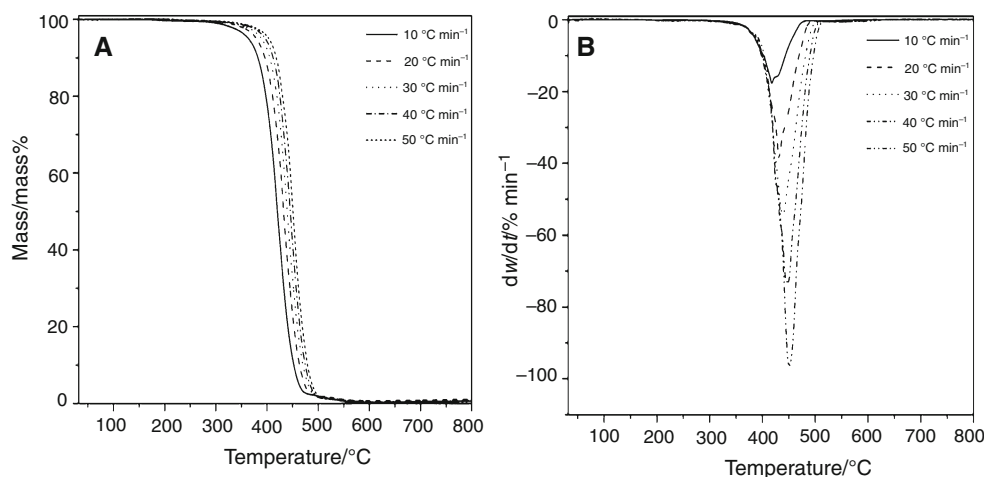


Table 1 Onset, endset and peak temperatures and their respective maximum mass loss of WCO

Heating rate/ °C min ⁻¹	T _o / °C	T _i /°C	M _{max} / mass%	T _{max} / °C	R ₅₀ / mass% min ⁻¹
10	318.7	478.7	- 17.56	418.5	- 17
20	339.8	484.2	- 38.65	431.5	- 38.5
30	347.7	490.1	- 54.17	438	- 54
40	356.6	492.5	- 73.08	449	- 73
50	362.4	496.6	- 96.15	452	- 96.5

the average activation energy values calculated for all kinetic methods (FM, KAS and FWO) were in good agreement. Thus, the models might be reliable for fitting the thermal degradation of WCO.

Thermal cracking of waste cooking oil (WCO) using semi-batch reactor

TGA profile of WCO sample (Fig. 2a) confirmed that the active decomposition of WCO occurred in the temperature range of 318–500 °C. Therefore, the laboratory-scale

cracking of WCO in a semi-batch reactor was conducted in the temperature range of 400–500 °C with 25 °C increment. The effect of cracking temperatures (400–500 °C), heating rates (10–20 °C min⁻¹) and residence time (60–300 min) on the yield of OLP was investigated. From Fig. 4, it can be observed that as the residence time increases from 60 to 180 min the yield of OLP increased for all the temperature ranges (400–500 °C) and heating rates (10–20 °C min⁻¹). Further, increase in the residence time to 300 min caused the increase in the yield of OLP for 400, 425 and 450 °C temperatures. However, increase in residence time to 300 min did not show significant enhancement in the yield of OLP at higher temperatures of 475 and 500 °C at both heating rates of 10 and 20 °C min⁻¹. This is may be due to secondary cracking of products at higher temperatures [32]. Figure 4a shows the effect of residence time on the yield of OLP for various temperatures at a heating rate of 10 °C min⁻¹. The OLP yield found to be increased from 8 to 29 mass% (400 °C), 12 to 51 mass% (425 °C), 18 to 64 mass% (450 °C), 28 to 74 mass% (475 °C) and 38 to 65 mass% (500 °C) with an increase in the residence time from 60 to 300 min at a

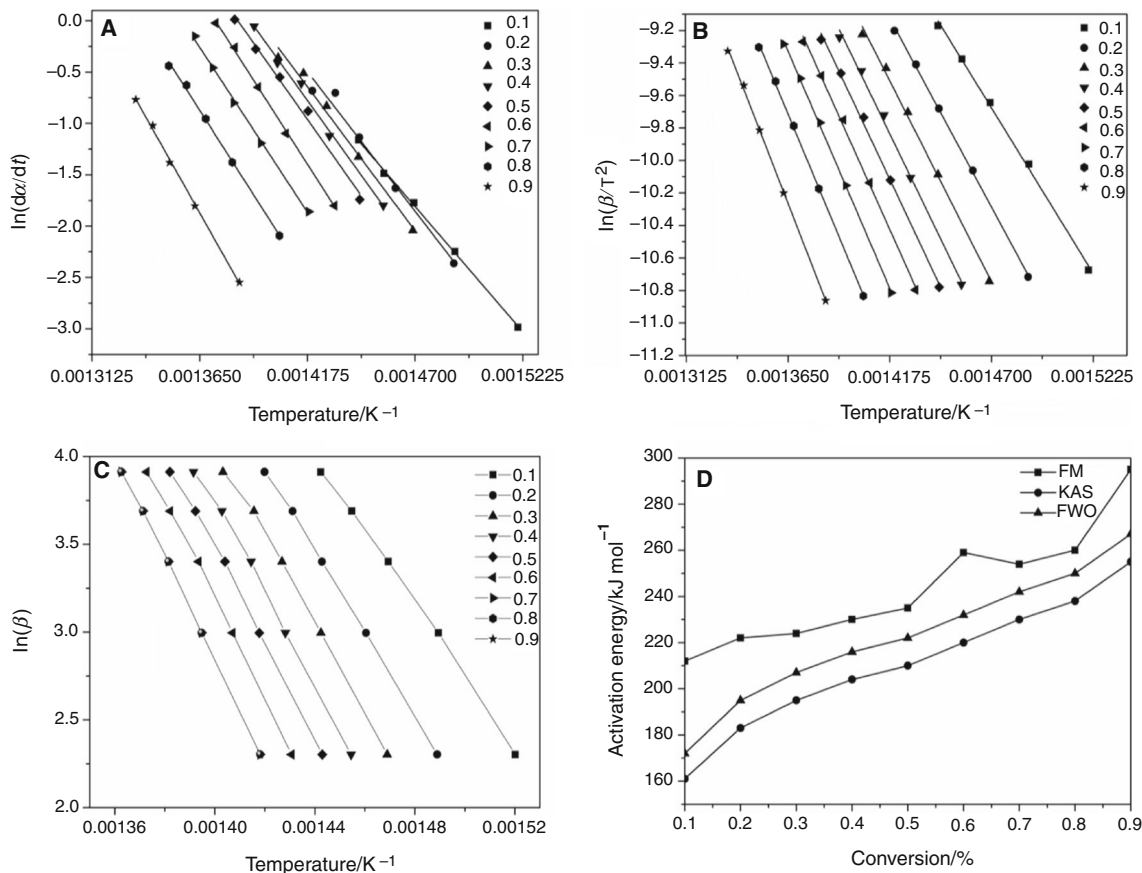
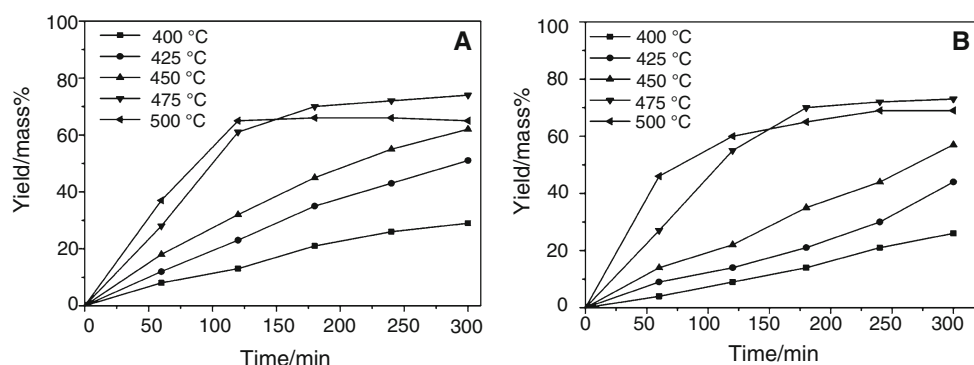


Fig. 3 Kinetic fitting of WCO degradation by FM (a), KAS (b), FWO (c) and activation energy distribution (d)

Table 2 Values of activation energies obtained using FM, FWO and KAS methods

FM			FWO			KAS		
α	$E/\text{kJ mol}^{-1}$	R^2	α	$E/\text{kJ mol}^{-1}$	R^2	α	$E/\text{kJ mol}^{-1}$	R^2
0.1	212.5	0.9946	0.1	172	0.9977	0.1	161	0.997
0.2	222.6	0.9951	0.2	195	0.9991	0.2	183.8	0.999
0.3	224	0.9994	0.3	207	0.9957	0.3	195.7	0.996
0.4	230.4	0.9970	0.4	216	0.9960	0.4	204.6	0.995
0.5	235.4	0.9895	0.5	222	0.9971	0.5	210.4	0.997
0.6	259	0.9984	0.6	232	0.9974	0.6	220.8	0.997
0.7	254	0.9972	0.7	242	0.9992	0.7	230.8	0.999
0.8	260	0.9973	0.8	250	0.9993	0.8	238	0.999
0.9	295	0.9981	0.9	267	0.9991	0.9	255.4	0.999
Avg. 243.7			Avg. 222			Avg. 211.3		

**Fig. 4** Effect of time on yield of OLP for heating rates of $10\text{ }^{\circ}\text{C min}^{-1}$ (a) and $20\text{ }^{\circ}\text{C min}^{-1}$ (b)

heating rate of $10\text{ }^{\circ}\text{C min}^{-1}$. From Fig. 4a, it can be seen that the OLP yield was increased continuously from 8 to 29, 12 to 51 and 18 to 63 mass% at cracking temperature of 400, 425 and 450 $^{\circ}\text{C}$, respectively, with an increase in the residence time from 60 to 300 min at a heating rate of $10\text{ }^{\circ}\text{C min}^{-1}$. However, the OLP yield was increased from 28 to 60 mass% (475 $^{\circ}\text{C}$) and 38 to 61 mass% (500 $^{\circ}\text{C}$) for the residence time of 60–120 min and further the OLP yield slightly increased in case of longer residence time and higher cracking temperatures (475 and 500 $^{\circ}\text{C}$). Similarly, for $20\text{ }^{\circ}\text{C min}^{-1}$ the yield of OLP was increased from 4 to 26 mass% (400 $^{\circ}\text{C}$), 9 to 44 mass% (425 $^{\circ}\text{C}$), 14 to 57 mass% (450 $^{\circ}\text{C}$), 27 to 72 mass% (475 $^{\circ}\text{C}$) and 46 to 65 mass% (500 $^{\circ}\text{C}$) as residence time increases from 60 to 300 min. Furthermore, from this study, it is concluded that for all studied cracking temperatures (i.e., 400–500 $^{\circ}\text{C}$), the higher yield of OLP was obtained at a heating rate of $10\text{ }^{\circ}\text{C min}^{-1}$ as compared to $20\text{ }^{\circ}\text{C min}^{-1}$. These results attribute that high heating rates favor the yield of non-condensable gases [33]. The values of the yield of OLP

obtained during thermal cracking of WCO were comparable with thermal cracking of soybean oil [34, 35] and rapeseed oil [36]. Overall, the optimum yield of 72 mass% of OLP was obtained at a residence time of 180 min and thermal cracking temperature of 475 $^{\circ}\text{C}$ at a heating rate of $10\text{ }^{\circ}\text{C min}^{-1}$.

Characterization of WCO and OLP

During thermal cracking of WCO, several reactions such as decarbonylation (CO removal), decarboxylation (CO_2 removal) and dehydration (H_2O removal) were observed which resulted in the formation of CO_2 , CO and H_2O as evolved products [37]. As a result, the ratio of carbon to oxygen atoms is higher in OLP as compared to WCO. For this reason, the higher calorific value was attained for OLP (39.25 MJ kg^{-1}) as compared to WCO (38.9 MJ kg^{-1}). The density of WCO and OLP was found to be 0.96 and 0.86 g cm^{-3} , respectively. The decrease in density (0.86 g cm^{-3}) and viscosity ($3.79\text{ mm}^2\text{ s}^{-1}$) of the

Table 3 Main chemical compounds present in OLP

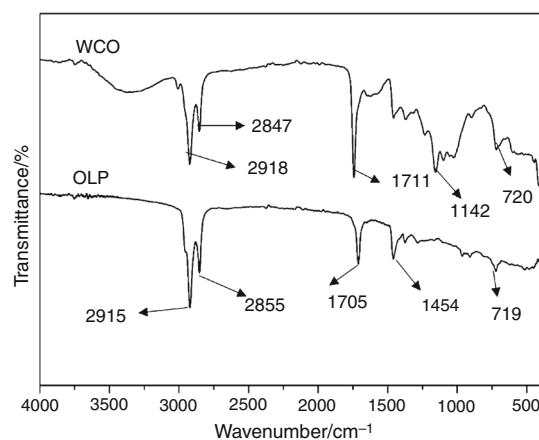
No.	RT/ min	Area/ %	Compounds	Formula
1	3.626	0.51	Oxirane, 2-methyl-3-(1-methylethyl)-	C ₆ H ₁₂ O
2	5.795	0.96	3-Hepten-1-ol 1-Undecyne	C ₇ H ₁₄ O C ₁₁ H ₂₀
3	6.595	1.23	Cyclopentene, 3-propyl	C ₈ H ₁₄
4	7.101	1.4	<i>o</i> -Xylene	C ₈ H ₁₀
5	7.816	2.18	3,4-Octadiene, 7-methyl 3-None Cyclopentene, 1-butyl Cyclopentene, 1-pentyl	C ₉ H ₁₆ C ₉ H ₁₆ C ₉ H ₁₆ C ₁₀ H ₁₈
6	10.120	2.4	Benzene, 1,2-diethyl Benzene, 1,3-diethyl Benzene, 1,4-diethyl	C ₁₀ H ₁₄ C ₁₀ H ₁₄ C ₁₀ H ₁₄
7	11.350	3.45	1-Ethylcyclopentene Cyclopentene, 3-propyl Cyclopentene, 3-ethyl 1-Ethylcyclopentene	C ₇ H ₁₂ C ₈ H ₁₄ C ₇ H ₁₂ C ₇ H ₁₂
8	12.340	0.43	2-Tetradecanone 2-Dodecanone 2-Tetradecanone 2-Undecanone	C ₁₄ H ₂₈ O C ₁₂ H ₂₄ O C ₁₄ H ₂₈ O C ₁₁ H ₂₂ O
9	13.383	0.36	Nonanoic acid	C ₉ H ₁₈ O ₂
10	13.703	0.32	7-Tetradecene 6-Dodecene, (E)-	C ₁₄ H ₂₈ C ₁₂ H ₂₄
11	13.836	2.1	Heptadecane, 2-methyl	C ₁₈ H ₃₈
12	14.413	0.16	1H-Indene, 1-ethylidene Naphthalene, 1-methyl Naphthalene, 2-methyl	C ₁₁ H ₁₀ C ₁₁ H ₁₀ C ₁₁ H ₁₀
13	15.103	2.78	7-Tetradecene	C ₁₄ H ₂₈
14	16.506	1.28	Dodecane, 2,6,10-trimethyl	C ₁₅ H ₃₂
15	24.510	0.97	9,12-Octadecadien-1-ol, (Z,Z)- 9,12-Octadecadienoic acid, methyl ester, (E,E)-	C ₁₈ H ₃₄ O C ₁₉ H ₃₄ O ₂

produced OLP were due to the removal of oxygen and cracking of higher molecular weight triglyceride of WCO into smaller molecules. The viscosity values were found to be in the range of those reported in the literature [38, 39]. The density of OLP obtained from thermal cracking of WCO was similar with OLP obtained from carinata oil (0.86 g cm⁻³) [40]. However, the density of OLP (0.86 g cm⁻³) estimated in the present study was lower than OLP (0.88 g cm⁻³) reported by Li et al. [39]. Moreover, the flash point is the lowest temperature at which the sample evaporates enough fluid to form a combustible gas. It indicates easy burning of the sample in air. It can be

claimed that the flash point of OLP obtained in this study was measured by ASTM standards and found to be 97 °C.

After the collection of condensable liquid during the cracking reactions, the collected OLP was subjected to GC-MS and FTIR analysis for identification of hydrocarbon fractions depending on their boiling range, i.e., gasoline (60–80 °C), kerosene (80–120 °C) and diesel (120–200 °C) fractions [41]. From GC-MS analysis of OLP shown in Table 3, it can be observed that the identified fraction contains hydrocarbon chains compounds between C₆ and C₁₉. Majority of hydrocarbon fractions found in this study ranges from C₇ to C₁₄. This study confirms the absence of aromatic hydrocarbons, olefinic and paraffinic hydrocarbons which were found to be the dominating fractions, and the results are comparable to those reported in the literature [42].

From Fig. 5, the FTIR spectra of WCO and OLP are found to be approximately similar which could be due to the similar nature of the chemical structure of functional groups present in the sample. But, only the characteristic peak at 1142 cm⁻¹ which represents a stretching vibration of C–O ester functional group in WCO sample. Symmetric (C–H) and asymmetric stretching of the saturated C–C bond was observed at wavenumber 2915–2918 and 2847–2855 cm⁻¹ for both samples, respectively. The stretching vibration at 1454 cm⁻¹ corresponds to bending vibrations of CH₂ and CH₃ aliphatic groups. The band at 719–720 cm⁻¹ belongs to the overlapping of methylene (–CH₂) rocking vibration and to the out-of-plane vibration of *cis*-disubstituted olefins [43]. Ester carbonyl functional group of the esters of glycerol (triglycerides) in WCO and fatty acid of esters in OLP sample were represented at 1705–1711 cm⁻¹. Similar observation was reported for waste palm cooking oil and rapeseed oil [43, 44]. From the overall FTIR spectra, it was observed that OLP contains

**Fig. 5** FTIR analysis of WCO and OLP

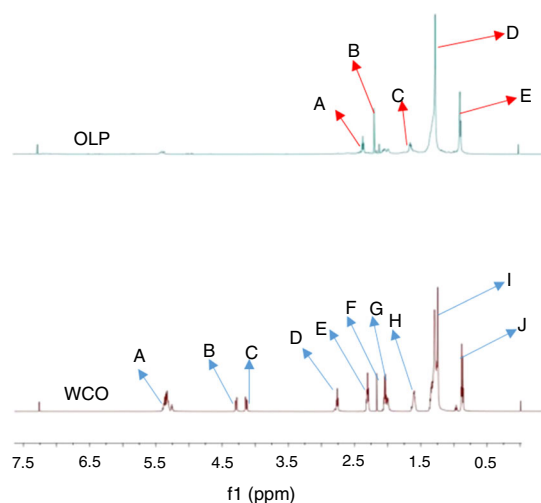


Fig. 6 ^1H NMR of WCO and OLP (Notations for A–J shown in Table 4)

Table 4 Relative hydrogen distributions in OLP

Samples	Chemical shift/ppm	Type of hydrogen
WCO	A	Unsaturated fatty acids of olefinic proton and glycerol
	B	$-\text{CH}_2\text{OCOR}$ (methylene protons (glycerol))
	C	Glycerol $(\text{CH}_2\text{O})(\alpha)$
	D	$=\text{HC}-\text{CH}_2-\text{CH}=\text{}$ (divinyl methylene protons)
	E	α -Carbonyl methylene protons
	F & G	Allylic protons ($-\text{C}=\text{C}-\text{CH}_2-\text{C}=\text{C}-$) and β -carbonyl methylene protons
	H	Methylene terminal including all acyl chains
	I	Saturated $(\text{CH}_2)_n$ groups
	J	$-\text{CH}_3$ primary alkyl protons
	OLP	A
B		Unsaturated fatty acids ($\text{CH}_2-\text{CH}=\text{CH}$)
C		β -Carbonyl methylene protons
D		Saturated $(\text{CH}_2)_n$ groups
E		Methyl protons

essential functional groups which confirm that the product comprises aliphatic hydrocarbons.

The chemical shifts and the relative hydrogen distributions in WCO and OLP obtained from ^1H NMR spectroscopy of the samples (Fig. 6) are listed in Table 4. The chemical shift regions for ^1H NMR can be grouped into three major regions: aromatic (9–6 ppm), olefinic

(6–4 ppm) and aliphatic (3–0.5 ppm) fractions [45, 46]. However, the aliphatic proton section has been further subdivided into $\text{H}\alpha$ (2–3 ppm), $\text{H}\beta$ (1–2 ppm) and $\text{H}\gamma$ regions (0.5–1 ppm). Table 4 signifies that both WCO and OLP did not contain fractions which belong to the aromatic range. Most of the characteristics peaks were in the range of 5–1 ppm for WCO and 2.5–0.76 ppm for OLP. In the ^1H NMR spectrum of OLP, chemical shifts between 0.76 and 1.38 ppm indicate hydrogen bonded to carbon, which confirmed the existence of aliphatic hydrocarbons, as well as the chemical shifts between 2.12 and 2.40 ppm indicate the presence of hydrogen and unsaturated fatty acids ($=\text{CH}-$ methine) groups, respectively. From the overall study of ^1H NMR, the dominating chemical shifts for OLP indicated that all the compounds in the sample correspond to aliphatic hydrocarbons and some traces of aliphatic carbonyl hydrocarbons.

Conclusions

The application of WCO for biofuel production would be a promising option to secure future energy demands. Moreover, the thermal kinetics and thermal cracking are the complementary studies in the present work. The TGA graph clarifies that with an increase in heating rates, the maximum mass loss rate increased and moved toward higher temperatures. From the graph, the sample described decomposition peak profiles that confirmed single decomposition stage and the main decomposition temperature was established between 318 and 500 $^\circ\text{C}$ in which more than 96.7 mass% of the sample was completely decomposed. Results obtained from TGA were used for activation energy calculation by non-isothermal, model-free kinetic methods such as FM, KAS and FWO within the conversion range of 0.1–0.9 from the slope of the lines. The activation energy obtained for WCO by FM, KAS and FWO was 243.7, 211.23, and 222 kJ mol^{-1} , respectively. From the result, it can be claimed that these methods were in good agreement and can be used to estimate the activation energy of WCO degradation. Further, thermal cracking of WCO oil was performed at a temperature range of 400–500 $^\circ\text{C}$ in which the optimum yield of 72 mass% OLP was obtained at a temperature of 475 $^\circ\text{C}$, with a heating rate of 10 $^\circ\text{C min}^{-1}$ and residence time of 180 min. It has been observed from ^1H NMR to GC–MS that the majority of fractions present in OLP corresponds to aliphatic hydrocarbons.

Acknowledgements The authors gratefully acknowledge Indian Institute of Technology Guwahati, Department of Chemical Engineering and Centre for Instrument Facility (CIF) for the provision of analytical facilities to carry out the research work.

References

- Santos AG, Caldeira VP, Farias MF, Araújo AS, Souza LD, Barros AK. Characterization and kinetic study of sunflower oil and biodiesel. *J Therm Anal Calorim*. 2011;106:747–51.
- Ong YK, Bhatia S. The current status and perspectives of biofuel production via catalytic cracking of edible and non-edible oils. *Energy*. 2010;35:111–9.
- Abdullah NH, Hasan SH, Yusoff NRM. Biodiesel production based on waste cooking oil (WCO). *Int J Comput Mater Sci Eng*. 2013;1:94–9.
- Taufiqurrahmi N, Bhatia S. Catalytic cracking of edible and non-edible oils for the production of biofuels. *Energy Environ Sci*. 2011;4:1087–112.
- Demirbas A. Progress and recent trends in biofuels. *Prog Energy Combust Sci*. 2007;33:1–18.
- Goyal H, Seal D, Saxena R. Bio-fuels from thermochemical conversion of renewable resources: a review. *Renew Sustain Energy Rev*. 2008;12:504–17.
- Hua T, Chunyi L, Chaohe Y, Honghong S. Alternative processing technology for converting vegetable oils and animal fats to clean fuels and light olefins. *Chin J Chem Eng*. 2008;16:394–400.
- Silva AAL, Oliveira DS, Fernandes FRD, Santos AGD, Caldeira VPS, Souza LD. Catalytic cracking of sunflower oil under Zr catalysts using thermogravimetry. *J Therm Anal Calorim*. 2017. doi:10.1007/s10973-017-6202-y.
- Rajeshwar K. The kinetics of the thermal decomposition of green river oil shale kerogen by non-isothermal thermogravimetry. *Thermochim Acta*. 1981;45:253–63.
- Torrente M, Galan M. Kinetics of the thermal decomposition of oil shale from *Puertollano* (Spain). *Fuel*. 2001;80:327–34.
- Kok MV. Thermal investigation of Seyitomer oil shale. *Thermochim Acta*. 2001;369:149–55.
- Karabakan A, Yürüm Y. Effect of the mineral matrix in the reactions of oil shales. *Fuel*. 1998;7:1303–9.
- Jaber J, Probert S. Non-isothermal thermogravimetry and decomposition kinetics of two Jordanian oil shales under different processing conditions. *Fuel Process Technol*. 2000;63:57–70.
- Reshad AS, Tiwari P, Goud VV. Thermal decomposition and kinetics of residual rubber seed cake and shell. *J Therm Anal Calorim*. 2017;129:577–92.
- Leroy V, Cancellieri D, Leoni E, Rossi JL. Kinetic study of forest fuels by TGA: model-free kinetic approach for the prediction of phenomena. *Thermochim Acta*. 2010;497:1–6.
- Mominou N, Xian S, Jiaoliang X. Studies on coprocessing vacuum residue oil with plastics using thermogravimetric analysis. *Pet Sci Technol*. 2009;27:588–96.
- Gornicka B, Gorecki L. TGA/DTG/DSC investigation of thermal ageing effects on polyamide-imide enamel. *J Therm Anal Calorim*. 2010;101:647–50.
- López F, Mercê A, Alguacil F, López-Delgado A. A kinetic study on the thermal behavior of chitosan. *J Therm Anal Calorim*. 2007;91:633–9.
- Sułkowski W, Danch A, Moczyński M, Radoń A, Sułkowska S, Borek J. Thermogravimetric study of rubber waste-polyurethane composites. *J Therm Anal Calorim*. 2004;78:905–21.
- Freire L, Bicudo T, Rosenhaim R, Sinfrônio F, Botelho J, Carvalho Filho J, et al. Thermal investigation of oil and biodiesel from *Jatropha curcas* L. *J Therm Anal Calorim*. 2009;96:1029–33.
- Coats AW, Redfern J. Kinetic parameters from thermogravimetric data. *Nature*. 1964;201:68–9.
- Doyle C. Kinetic analysis of thermogravimetric data. *J Appl Polym Sci*. 1961;5:285–92.
- Lee T, Beck S. A new integral approximation formula for kinetic analysis of nonisothermal TGA data. *AIChE J*. 1984;30:517–9.
- Flynn JH, Wall LA. A quick, direct method for the determination of activation energy from thermogravimetric data. *J Polym Sci*. 1966;4:323–8.
- Ozawa T. A new method of analyzing thermogravimetric data. *Bull Chem Soc Jpn*. 1965;38:1881–6.
- Kissinger HE. Reaction kinetics in differential thermal analysis. *Anal Chem*. 1957;29:1702–6.
- Friedman HL. Kinetics of thermal degradation of char-forming plastics from thermogravimetry. *J Polym Sci*. 1964;6:183–95.
- Volli V, Purkait M. Physico-chemical properties and thermal degradation studies of commercial oils in nitrogen atmosphere. *Fuel*. 2014;117:1010–9.
- Borugadda VB, Goud VV. Biodiesel production from renewable feedstocks: status and opportunities. *Renew Sustain Energy Rev*. 2012;16:4763–84.
- Alptekin E, Canakci M. Determination of the density and the viscosities of biodiesel–diesel fuel blends. *J Renew Energy*. 2008;33:2623–30.
- Słopiecka K, Bartocci P, Fantozzi F. Thermogravimetric analysis and kinetic study of poplar wood pyrolysis. *Appl Energy*. 2012;97:491–7.
- Taufiqurrahmi N, Mohamed AR, Bhatia S. Production of biofuel from waste cooking palm oil using nanocrystalline zeolite as catalyst: process optimization studies. *Bioresour Technol*. 2011;102:10686–94.
- Nazzal JM. Influence of heating rate on the pyrolysis of Jordan oil shale. *J Anal Appl Pyrolysis*. 2002;62:225–38.
- Lima DG, Soares VC, Ribeiro EB, Carvalho DA, Cardoso EC, Rassi FC, et al. Diesel-like fuel obtained by pyrolysis of vegetable oils. *J Anal Appl Pyrolysis*. 2004;71:987–96.
- Wiggers V, Meier H, Wisniewski A, Barros AC, Maciel MW. Biofuels from continuous fast pyrolysis of soybean oil: a pilot plant study. *Bioresour Technol*. 2009;100:6570–7.
- Onay O, Koçkar OM. Pyrolysis of rapeseed in a free fall reactor for production of bio-oil. *Fuel*. 2006;85:1921–8.
- Lestari S, Mäki-Arvela P, Beltramini J, Lu G, Murzin DY. Transforming triglycerides and fatty acids into biofuels. *ChemSuschem*. 2009;2:1109–19.
- Lin YF, Wu YP, Chang CT. Combustion characteristics of waste-oil produced biodiesel/diesel fuel blends. *J Fuels*. 2007;86:1772–80.
- Li L, Ding Z, Li K, Xu J, Liu F, Liu S, et al. Liquid hydrocarbon fuels from catalytic cracking of waste cooking oils using ultra-stable zeolite USY as catalyst. *J Anal Appl Pyrolysis*. 2016;117:268–72.
- Zhao X, Wei L, Cheng S, Cao Y, Julson J, Gu Z. Catalytic cracking of carinata oil for hydrocarbon biofuel over fresh and regenerated Zn/Na-ZSM-5. *Appl Catal*. 2015;507:44–55.
- Gary J, Handwerk G. *Petroleum refining technology and economics*. 4th ed. New York: Marcel Dekker Inc.; 2001.
- Mota SD, Mancio A, Lhamas D, Abreu DD, Silva MD, Santos WD, et al. Production of green diesel by thermal catalytic cracking of crude palm oil (*Elaeis guineensis Jacq*) in a pilot plant. *J Anal Appl Pyrolysis*. 2014;110:1–11.
- Ullah Z, Bustam MA, Man Z. Characterization of waste palm cooking oil for biodiesel production. *Int J Chem Eng Appl*. 2014;5:134–7.
- Qiu F, Li Y, Yang D, Li X, Sun P. Biodiesel production from mixed soybean oil and rapeseed oil. *Appl Energy*. 2011;88:2050–5.
- Monteiro MR, Ambrozini ARP, et al. Evaluation of biodiesel–diesel blends quality using ¹H NMR and chemometrics. *Talanta*. 2009;78:660–4.
- Şensöz S, Demiral I, Gerçel HF. Olive bagasse (*Olea europaea* L.) pyrolysis. *Bioresour Technol*. 2006;97:429–36.